

# RAC: Rectified Flow Auto Coder

Sen Fang<sup>1</sup>, Yalin Feng<sup>2\*</sup>, Yanxin Zhang<sup>3</sup>, and Dimitris N. Metaxas<sup>1</sup>

<sup>1</sup> Rutgers University, Piscataway NJ, USA

<sup>2</sup> Nanyang Technological University, Singapore

<sup>3</sup> University of Wisconsin-Madison, Madison WI, USA

\*Equal contribution

<https://world-snapshot.github.io/RAC>

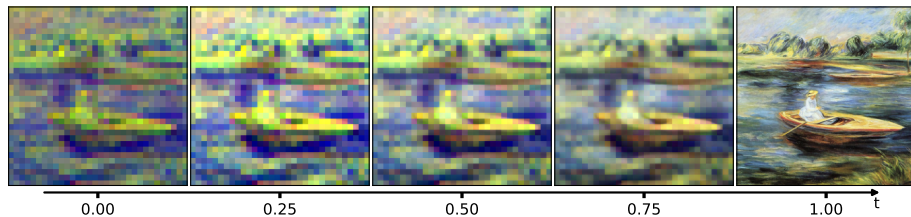


**Fig. 1: The trajectory demonstration of RAC:** Make the reconstruction task a condition generation task; Make the decoder the encoder; Make the single-step decoding and encoding a multi-step decoding and encoding.

**Abstract.** In this paper, we propose a **Rectified Flow Auto Coder (RAC)** inspired by Rectified Flow to replace the traditional VAE: **1.** It achieves multi-step decoding by applying the decoder to flow timesteps. Its decoding path is straight and correctable, enabling step-by-step refinement. **2.** The model inherently supports bidirectional inference, where the decoder serves as the encoder through time reversal (hence *Coder* rather than encoder or decoder), reducing parameter count by nearly 41%. **3.** This generative decoding method improves generation quality since the model can correct latent variables along the path, partially addressing the reconstruction-generation gap. Experiments show that RAC surpasses SOTA VAEs in both reconstruction and generation with approximately 70% lower computational cost.

**Keywords:** Rectified Flow · Flow Matching · Variational Autoencoder

## 1 Introduction

In the field of generative models, over the past many years, there has been a problem of inconsistent generation and reconstruction results. For instance, when using the same generation method and the same VAE, the generation results are often inferior to the reconstruction results: **(1)** Some studies consider it to be a problem of representation [29, 35], and attempt to solve it by optimizing the latent space; **(2)** Some studies consider it to be a problem of training strategy [15], and use the generation backbone and VAE for joint training optimization; **(3)** Some studies consider it to be a problem of the method [36], and propose a native unified method to try to solve it, etc.

arXiv:2603.05925v1 [cs.CV] 6 Mar 2026

Under the same conditions of using VAE [10], one very obvious and unique variable that distinguishes generation from reconstruction is - the variables used during generation are provided by the generation framework (such as Unet, DiT, etc.). Therefore, we hypothesize that part of the reason is that the latent variables output by the generation method are problematic. **It easily misses the uneven manifold space of traditional VAE**, resulting in unstable generation effects and being less accurate than the encoder provided by VAE itself<sup>4</sup>.

So, in the case of minimal modifications, the method to enhance the decoder’s performance during generation is to incorporate the decoder into the generation process. As shown in Fig. 1, we introduce the concepts of time steps and velocity fields into the decoder, **enabling it to gradually calibrate the input variables or the behavior during encoding**, and theoretically, it inherently supports bidirectional transformation. The decoder of traditional VAE is an important part of the generation process. Generation frameworks (such as Unet [23], DiT [19], etc.) can perform multi-step reasoning, but the end VAE is actually a one-step generation. This is actually not very reasonable: Consider a navigator who, despite having a correctable route, is forced to teleport directly to the destination in one step — losing all opportunity to adjust course along the way.

Specifically, we take a unified view of continuous-time generation and representation learning, and elevate the classic VAE decoder from a pointwise mapping to a *path-level* generative process: a time-conditioned velocity field defines an integrable flow from latent variables to the image space, and explicitly models a correctable, multi-step decoding trajectory. This design provides a structured generation path while making the same model naturally act as an encoder under time reversal, enabling parameter sharing and bidirectional consistency. For training, we center on path consistency, latent alignment, and reconstruction constraints, yielding a unified optimization framework that balances invertibility and generation quality. Our contributions are threefold:

- We propose RAC, which generalizes VAE decoding from a *single-step map* to a *continuous-time, integrable path*, establishing a **unified flow-based autoencoding paradigm** for generation and representation.
- We design a **structured bidirectional mechanism** where the same velocity-field model performs decoding and encoding in forward and reverse time, achieving parameter sharing, path reversibility, and generation–reconstruction consistency.
- We present a stable training objective and implementation recipe (**path consistency + latent alignment + reconstruction constraints**, with optional mean-velocity regularization), delivering strong reconstruction and generation performance at comparable model scale.

---

<sup>4</sup> From another perspective, Text2Img (prediction, information increase) is not as precise as Img2Latent (encoding compression, information reduction), which can also serve as a reason for the disparity in the generation and reconstruction capabilities.

## 2 Related Work

### 2.1 Flow-Based Generative Models

Normalizing flow models [34] learn invertible mappings between complex data distributions and simple priors. Early works such as Real NVP [3] and Glow [11] establish the foundation of flow-based generation by enabling tractable likelihood estimation through invertible transformations. Recent studies extend flow models toward diffusion-inspired formulations. Flow Matching (FM) [16] and Rectified Flow (RF) [17] reformulate diffusion training as direct vector field regression, enabling deterministic sampling and efficient training. These methods bridge continuous normalizing flows [1,9,26] and diffusion models [21,24], achieving competitive generation quality with reduced sampling steps.

### 2.2 Variational Autoencoders and Representation Learning

Variational Autoencoders (VAEs) [10] provide a principled framework for learning latent-variable generative models via variational inference. However, standard VAEs often suffer from posterior collapse and limited reconstruction fidelity. To alleviate these issues, Representations Autoencoders (RAEs) [35] replace KL regularization with explicit latent constraints. Sparse Autoencoders (SAEs) [25] enforce sparsity priors to promote compact and interpretable representations.

Recent advances focus on improving latent expressiveness and generative performance. REPA-E [15] introduces residual posterior alignment for end-to-end latent diffusion training. TAESD [4] adopts vector-quantized autoencoders for efficient latent generative modeling. Hybrid diffusion-autoencoder frameworks [30] further improve inference and generation consistency. NVAE [28] proposes hierarchical latent variables for scalable high-resolution synthesis. These approaches demonstrate that carefully designed latent regularization and architectural constraints are crucial for balancing reconstruction quality and generative diversity.

### 2.3 Unified Modeling of Generation and Reconstruction

Recent research explores unifying generation and reconstruction within a single probabilistic framework. Latent diffusion models [21] combine autoencoding architectures with diffusion processes for efficient high-resolution synthesis.

Several works interpret autoencoding and sampling as two sides of the same stochastic process. Score-based models [27] and flow matching methods [16] naturally support both data reconstruction and generation via conditional sampling. Consistency models [26] further enable fast bidirectional mappings.

Recent end-to-end latent learning frameworks [5–8, 15, 29] explicitly couple inference and generation modules, improving representation alignment and robustness. Such unified designs facilitate efficient downstream adaptation and controllable synthesis. Our work follows this line of research by jointly modeling reconstruction and generation within a unified flow-based latent framework, achieving improved fidelity and sampling efficiency.

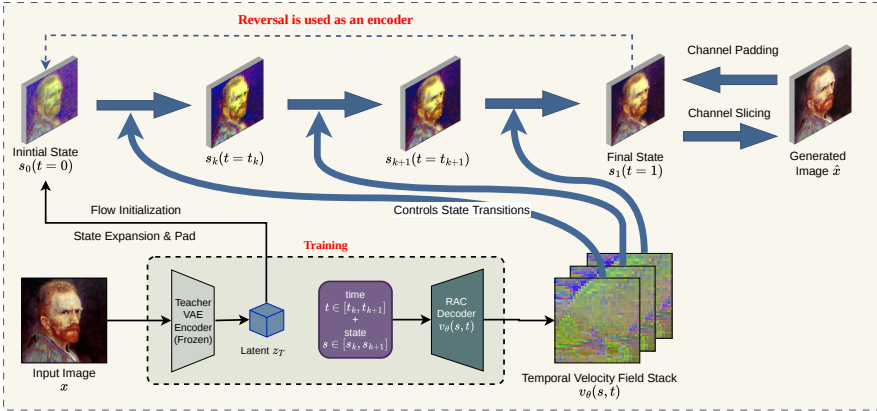


**Fig. 2: Method Overview.** (i) **Training.** To prevent latent space collapse, we freeze the VAE encoder and train only the RAC decoder; reverse-time inference then serves as encoding. (ii) **State Construction.** Extra channels beyond RGB are padded with 0.5, keeping the velocity field shape constant and ensuring bidirectional consistency. (iii) **RAC Input.** RAC takes time  $t$  and the current state as input, driving the transition from latent initialization to the target image.

### 3 Methodology

Figure 2 illustrates the RAC pipeline. We replace the single-step VAE decoder with a continuous-time velocity field  $\mathbf{v}_\theta$ , which integrates a full-resolution *state* tensor  $\mathbf{s} \in \mathbb{R}^{C_s \times H \times W}$  from a latent-derived initialization to the target image state  $\mathbf{s}^*$ ; time-reversal of the same model performs encoding. To prevent latent space collapse, we freeze the VAE encoder and train only the decoder under a joint objective covering reconstruction, path consistency, and latent alignment.

#### 3.1 Overview and Goal

The core idea is to replace the single-step VAE decoder with a *time-conditioned velocity field*  $\mathbf{v}_\theta(\mathbf{s}, t)$  that integrates a *state*  $\mathbf{s}$  from a latent-derived initialization  $\mathbf{s}_0$  to a target image state  $\mathbf{s}^*$ ; running the same field in reverse serves as encoding. This formulation targets the fundamental mismatch in VAE-style models: reconstruction uses a data-conditioned encoder, while generation relies on latents that may not respect the decoder’s learned manifold. By making decoding a multi-step, correctable process, generation can actively refine latent variables along the path rather than committing to a one-shot projection.

Let  $\mathbf{x} \in [0, 1]^{3 \times H \times W}$  be an image and  $\tilde{\mathbf{x}} = 2\mathbf{x} - 1 \in [-1, 1]^{3 \times H \times W}$  its normalized version. We define a state tensor by padding channels:

$$\mathbf{s} = \text{pad}(\tilde{\mathbf{x}}) \in \mathbb{R}^{C_s \times H \times W}, \quad C_s \geq 3. \quad (1)$$

A KL-VAE teacher provides a latent target  $\mathbf{z}_T \in \mathbb{R}^{C \times h \times w}$ . Instead of a single-step decode, we learn a continuous-time flow from latent state to image state, and

reuse the same flow in reverse for encoding. This gives us a single model that (i) decodes with step-wise correction, (ii) supports bidirectional inference, and (iii) aligns generation and reconstruction within one mechanism. This formulation is intentionally generic: any KL-regularized VAE can serve as the teacher, which makes the method broadly compatible with existing pipelines.

### 3.2 Time-Conditioned Rectified Flow Decoder

We model the decoder as a time-conditioned velocity field:

$$\frac{ds(t)}{dt} = \mathbf{v}_\theta(\mathbf{s}(t), t), \quad t \in [0, 1]. \quad (2)$$

The velocity field is predicted by a lightweight VAE backbone [22]. To stabilize and structure the flow, we concatenate an explicit time channel and (optionally) a relative positional encoding. The network predicts velocities in the *downsampled* state space, which keeps the model compact and computation stable:  $\mathbf{v}_\theta(\mathbf{s}, t) = f_\theta(\text{down}(\mathbf{s}), t1, \text{pos}(\mathbf{s}))$ .

We build a latent state by padding the teacher latent and spatially expanding it:

$$\mathbf{s}_0 = \text{expand}(\text{pad}(\mathbf{z}_T)) \in \mathbb{R}^{C_s \times H \times W}. \quad (3)$$

Decoding is then performed by integrating the flow from  $t = 0$  to  $t = 1$ :

$$\mathbf{s}_1 = \mathbf{s}_0 + \int_0^1 \mathbf{v}_\theta(\mathbf{s}(t), t) dt, \quad (4)$$

and the predicted RGB image is the projection  $\hat{\mathbf{x}} = \Pi(\mathbf{s}_1)$  onto the first three channels. Crucially, the *same* model yields an encoder by reversing time:

$$\mathbf{s}_0 = \mathbf{s}_1 - \int_0^1 \mathbf{v}_\theta(\mathbf{s}(t), t) dt. \quad (5)$$

In practice we use  $K$  Euler steps with optional random time grids to encourage robustness:

$$\mathbf{s}_{k+1} = \mathbf{s}_k + \Delta t_k \mathbf{v}_\theta(\mathbf{s}_k, t_k), \quad k = 0, \dots, K - 1, \quad (6)$$

and inject small Gaussian noise per step to prevent brittle dynamics. This step-wise integration explicitly exposes intermediate states, enabling both diagnostic visualization and targeted regularization of the decoding path.

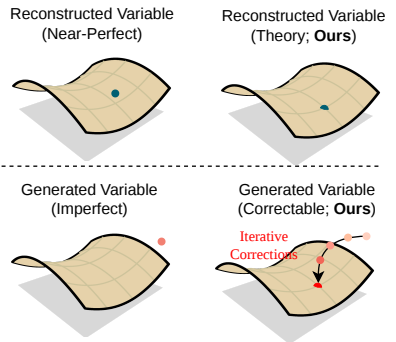


**Fig. 3: Reconstruction is Condition Generation:** The previous reconstructions were more accurate because they could relatively approach the manifold. The previous generations predicted variables that were often some distance away from the manifold. This is part of the reason for the past differences in the performance of generation and reconstruction. However, our method theoretically aims for perfect reconstruction, and the multi-step decoding can correct the potential variables provided by Unet or DiT. Therefore, both reconstruction and generation are significantly superior to traditional VAEs.

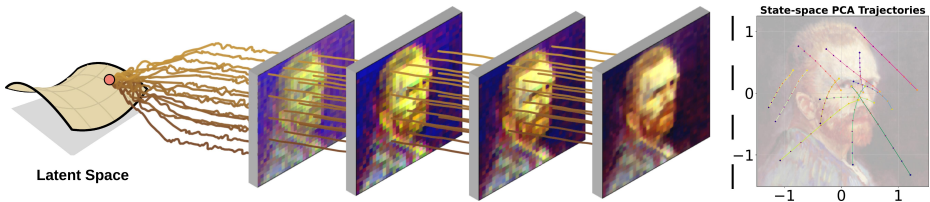


**Fig. 4: Conceptual and empirical views of RAC generation trajectories.** Left: a conceptual illustration of trajectory-based generation from latent space to image space. Right: sampled state trajectories projected into a 2D PCA space.

As shown in Figure 3, this method enables it to start by inherently knowing how to reconstruct through each image state, gradually learning to generate (construct a Latent Space), and then learning the multi-step calibration decoding process. That is to say, we have captured a more accurate learning objective for bridging generation and reconstruction.

### 3.3 State Construction and Transition

To bridge the resolution gap between latent space and image space, we introduce explicit *state construction* operators. The KL-VAE latent is padded and spatially expanded into a full-resolution latent state:

$$\mathbf{s}_0 = \text{expand}(\text{pad}(\mathbf{z}_T)) \in \mathbb{R}^{C_s \times H \times W}. \quad (7)$$

The target image state is defined by padding the normalized image:  $\mathbf{s}^* = \text{pad}(\tilde{\mathbf{x}})$ . The transition  $\mathbf{s}_0 \rightarrow \mathbf{s}^*$  is performed by integrating the rectified flow, producing a trajectory  $\{\mathbf{s}_k\}_{k=0}^K$ :

$$\mathbf{s}_{k+1} = \mathbf{s}_k + \Delta t_k \mathbf{v}_\theta(\mathbf{s}_k, t_k), \quad k = 0, \dots, K - 1. \quad (8)$$

The inverse transition is obtained by time reversal using the same velocity field, enabling a single-model encoder–decoder pair. This explicit state transition view makes the generation path interpretable and allows step-wise correction in both directions, which is particularly important when the generated latent deviates from the encoder manifold. The encoded full-resolution state is downsampled back to the teacher latent size via a lightweight learned projector or average pooling.

As shown in Fig. 4, RAC generation can be viewed as a trajectory-based process rather than a single-step mapping. The left panel provides an intuitive illustration of this perspective, where a latent representation evolves through a sequence of intermediate image states. The right panel offers an empirical counterpart by projecting sampled state trajectories into a 2D PCA space. These projected paths suggest that RAC follows structured and coordinated routes in its shared state space during generation.

### 3.4 Training Objectives

Our losses are designed to enforce three properties: *accurate reconstruction*, *rectified paths*, and *latent consistency*. Let  $\mathbf{s}^* = \text{pad}(\tilde{\mathbf{x}})$  be the target image state and  $\{\mathbf{s}_k\}_{k=0}^K$  the decoded trajectory. We define a standard reconstruction loss:  $\mathcal{L}_{\text{recon}} = \|\mathbf{s}_K - \mathbf{s}^*\|_2^2$ . To explicitly encourage a *uniform, correctable* path, we penalize deviation from linear interpolation:

$$\mathcal{L}_{\text{path}}^{\text{dec}} = \frac{1}{K-1} \sum_{k=1}^{K-1} \left\| \mathbf{s}_k - \left( \mathbf{s}_0 + \frac{k}{K} (\mathbf{s}^* - \mathbf{s}_0) \right) \right\|_2^2. \quad (9)$$

For encoding, we reverse the flow to obtain  $\hat{\mathbf{s}}_0$ , downsample it to latent  $\hat{\mathbf{z}}$ , and align it with the teacher latent:  $\mathcal{L}_{\text{latent}} = \|\hat{\mathbf{z}} - \mathbf{z}_T\|_2^2$ .

We further require that the teacher decoder applied to  $\hat{\mathbf{z}}$  matches the input image:  $\mathcal{L}_{\text{pixel}} = \|\text{Dec}_T(\hat{\mathbf{z}}) - \mathbf{x}\|_2^2$ . Finally, we enforce round-trip consistency so that encoding followed by decoding returns to the same image state:

$$\mathcal{L}_{\text{rt}} = \|\text{Flow}_\theta(\text{Flow}_\theta^{-1}(\mathbf{s}^*)) - \mathbf{s}^*\|_2^2. \quad (10)$$

Optionally, we add a mean-velocity regularizer inspired by rectified flow to stabilize time derivatives:

$$\mathcal{L}_{\text{mv}} = \left\| \mathbf{v}_\theta(\mathbf{s}(t), t) - (\mathbf{v} - t \partial_t \mathbf{v}) \right\|_2^2. \quad (11)$$

The final objective is:

$$\mathcal{L} = \mathcal{L}_{\text{recon}} + \lambda_{\text{path}} \mathcal{L}_{\text{path}}^{\text{dec}} + \lambda_{\text{latent}} \mathcal{L}_{\text{latent}} + \lambda_{\text{pixel}} \mathcal{L}_{\text{pixel}} + \lambda_{\text{rt}} \mathcal{L}_{\text{rt}} + \lambda_{\text{mv}} \mathcal{L}_{\text{mv}}. \quad (12)$$

These objectives jointly enforce accurate endpoints, rectified intermediate paths, and latent alignment, which is crucial for maintaining consistency between reconstruction and generation.

### 3.5 Algorithm and Implementation Details

We use a KL-VAE teacher for latent supervision, AdamW for optimization, and mixed precision to reduce memory. The same parameters are shared for forward and reverse flows, which keeps the model compact while enforcing bidirectional structure. A random time grid and step noise are used to avoid overfitting to fixed integration schedules.

**Default settings.** Unless otherwise noted, as show in Algorithm 1, we use  $K=4$  Euler steps,  $C_s=4$  state channels, AdamW with learning rate  $3 \times 10^{-4}$  and  $(\beta_1, \beta_2) = (0.9, 0.99)$ , input resolution 256, and a small step noise ( $\sigma = 0.05$ ). We enable random time grids during training and use mixed precision when available. The weights are typically set to  $\lambda_{\text{path}} = 0.1$ ,  $\lambda_{\text{latent}} = 1.0$ ,  $\lambda_{\text{pixel}} = 1.0$ , and  $\lambda_{\text{rt}} = 1.0$ .

---

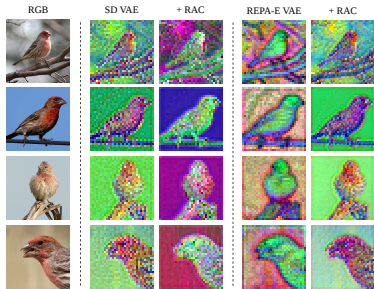
**Algorithm 1:** RAC Training (one iteration)

---

**Require:** image batch  $\mathbf{x}$ , teacher AE, steps  $K$

- 1:  $\tilde{\mathbf{x}} \leftarrow 2\mathbf{x} - 1$
- 2:  $\mathbf{z}_T \leftarrow \text{Enc}_T(\tilde{\mathbf{x}})$
- 3:  $\mathbf{s}_0 \leftarrow \text{expand}(\text{pad}(\mathbf{z}_T))$
- 4:  $\{\mathbf{s}_k\}_{k=0}^K \leftarrow \text{Flow}_\theta(\mathbf{s}_0)$
- 5:  $\mathbf{s}^* \leftarrow \text{pad}(\tilde{\mathbf{x}})$
- 6: compute  $\mathcal{L}_{\text{recon}}, \mathcal{L}_{\text{path}}^{\text{dec}}$
- 7:  $\hat{\mathbf{s}}_0 \leftarrow \text{Flow}_\theta^{-1}(\mathbf{s}^*)$
- 8:  $\hat{\mathbf{z}} \leftarrow \text{down}(\hat{\mathbf{s}}_0)$
- 9: compute  $\mathcal{L}_{\text{latent}}, \mathcal{L}_{\text{pixel}}, \mathcal{L}_{\text{rt}}$
- 10:  $\mathcal{L} \leftarrow \text{Eq.}(13)$ ; update  $\theta$  with AdamW

---



(a) PCA Analysis on VAE Latent Space Structure. We are cleaner.



(b) Performance Improvements with Baseline (400K Steps)

### Fig. 5: The State Space of RAC is a More Organized Representation Space.

(a) We used PCA to conduct a visual analysis of the state space that we encoded. This state space represents the state before the final output of the encoder. We can clearly observe that the training of RAC has made the original Latent representation more orderly and clean. (b) Comparison of gFID-50K on ImageNet  $256 \times 256$  [2] across different VAE configurations. We report results for the baseline methods (REPA [33], REPA-E [15, 22] and EQ-VAE [12]), comparing each against our approach trained under identical settings. Lower gFID-50K indicates better generation quality. RAC consistently outperforms the corresponding baselines across all VAE settings.

## 4 Experiments

In this section, we present a comprehensive evaluation of RAC, including reconstruction quality comparison (§4.1), generation quality comparison (§4.2), bidirectional consistency and parameter efficiency (§4.3), generation–reconstruction gap analysis (§4.4), ablation study (§4.5), and visualization evaluation (§4.6).

**Setup.** All the datasets used in our experiments are the same as those of the comparison models. The detailed experimental settings will be explained in the corresponding sections.

### 4.1 Reconstruction Quality

**Reconstruction Quality Comparison.** As visualized in Figure 5(a), the latent representations induced by RAC exhibit significantly cleaner and more coherent structures compared to the standard SD-VAE, which we attribute to the path consistency and latent alignment objectives jointly regularizing the state space during training. This structural regularity not only benefits generation—as reflected by the consistent gFID-50K improvements across all VAE configurations in Figure 5(b)—but also leads to more faithful image reconstruction, since a well-organized state space provides smoother and more stable ODE trajectories during the reverse decoding process. Quantitatively, RAC achieves competitive reconstruction quality while simultaneously improving generative performance, demonstrating that the two objectives are complementary rather than conflicting within our flow-based autoencoding framework.

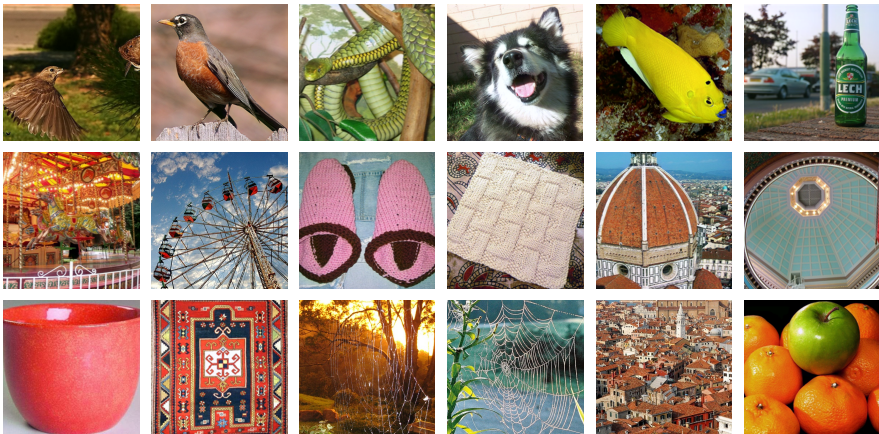
Autoencoder	gFID↓	sFID↓	IS↑	Prec.↑	Rec.↑	ΔParams	Decoder	rFID	GFLOPs
SD-VAE [22]	24.1	6.25	55.7	0.62	0.60	0.0%	SD-VAE-0.1x	0.44	94.3
+REPA-E [15]	16.3	5.69	75.0	0.68	0.60	0.0%	SD-VAE-0.2x	0.39	152.4
<b>+RAC (Ours)</b>	<b>14.8</b>	<b>5.43</b>	<b>78.3</b>	<b>0.70</b>	<b>0.61</b>	<b>-40.8%</b>	SD-VAE-0.3x	0.35	254.5
IN-VAE [15, 22]	22.7	5.47	56.0	0.62	0.62	0.0%	SD-VAE	0.62	310.4
+REPA-E [15]	12.7	5.57	84.0	0.69	0.62	0.0%			
<b>+RAC (Ours)</b>	<b>11.2</b>	<b>5.21</b>	<b>87.5</b>	<b>0.71</b>	<b>0.63</b>	<b>-40.7%</b>			
VA-VAE [31]	12.8	6.47	83.8	0.71	0.58	0.0%			
+REPA-E [15]	11.1	5.31	88.8	0.72	0.61	0.0%			
<b>+RAC (Ours)</b>	<b>9.8</b>	<b>5.08</b>	<b>91.4</b>	<b>0.73</b>	<b>0.62</b>	<b>-40.7%</b>			

**Scalable Decoders:** improve rFID while remaining much more efficient than VAEs. 0.1x indicates that the parameter being used is one-tenth of the SD.

**Table 1: Variation in VAE Architecture.** All baselines are reported using vanilla-REPA [33] for training. RACs consistently outperform baseline in reconstruction (rFID) on ImageNet-1K while being more efficient. Default settings are highlighted in gray.

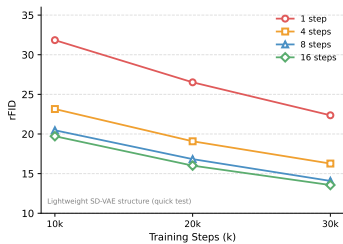
Table 1(a) presents a comprehensive comparison of generation quality across three VAE backbones—SD-VAE, IN-VAE, and VA-VAE—each evaluated under three training configurations: the vanilla baseline, +REPA-E, and our proposed +RAC. Across all metrics including gFID, sFID, IS, Precision, and Recall, RAC consistently achieves the best performance within each VAE group. For SD-VAE, RAC reduces gFID from 24.1 (baseline) to 14.8, outperforming the +REPA-E variant at 16.3, while also improving IS from 75.0 to 78.3. A similar trend holds for IN-VAE, where RAC achieves a gFID of 11.2 compared to 12.7 under REPA-E, alongside improvements in sFID and IS. For the strongest backbone VA-VAE, RAC further pushes gFID down to 9.8 from 11.1, with sFID improving from 5.31 to 5.08 and IS reaching 91.4. Finally, we presented the parameter changes of our RAC compared to the original VAE. It can be observed that the parameters have generally decreased by approximately 41%. These consistent gains across all three VAE configurations demonstrate that RAC is not tailored to a specific encoder architecture, but rather provides a general and complementary improvement on top of any pretrained VAE backbone, reinforcing the effectiveness of our flow-based autoencoding framework as a plug-in enhancement for latent training.

Table 1(b) examines how decoder scale affects reconstruction quality (rFID) and computational efficiency (GFLOPs) within the RAC framework. We evaluate three scaled decoder variants—SD-VAE-0.1x, SD-VAE-0.2x, and SD-VAE-0.3x—where the scale factor indicates the proportion of parameters retained relative to the full SD-VAE decoder, and compare against the full SD-VAE as reference. Despite using only a fraction of the original parameters, all three variants achieve substantially better rFID than the full SD-VAE: SD-VAE-0.1x already reaches 0.44 at just 94.3 GFLOPs, while SD-VAE-0.3x further improves to 0.35 at 254.5 GFLOPs, both surpassing the SD-VAE baseline of 0.62 at 310.4 GFLOPs. This reveals a counterintuitive but important finding: within the RAC decoding paradigm, a significantly smaller decoder not only reduces computational cost (approximately 70%) but also yields better reconstruction fidelity, suggesting that the continuous flow-based decoding path alleviates the representational burden traditionally placed on the decoder capacity, enabling high-quality reconstruction even under aggressive parameter reduction.



**Fig. 6: Qualitative Results on Imagenet  $256 \times 256$  using RAC.** It can achieve significant results in the state reconstruction mode with just 30k steps.

**Visual Reconstruction Comparison.** As shown in Fig. 6, RAC demonstrates strong qualitative reconstruction performance on ImageNet  $256 \times 256$  across a diverse range of visual categories, including animals, textures, architecture, and everyday objects, all within just 30k training steps. The reconstructed images faithfully preserve fine-grained details such as fur texture on the dog, the intricate scale patterns of the snake, the woven structure of the slippers, and the ornate geometric motifs of the carpet—details that are typically challenging for conventional VAE decoders operating under aggressive spatial compression. Beyond texture fidelity, RAC also maintains accurate global structure and color distribution, as evidenced by the sharp silhouette of the robin, the vivid green of the beer bottle, and the dome geometry of the Florence Cathedral.



**Fig. 7: rFID vs. Training Steps under Different Inference Steps.** Results on a lightweight SD-VAE structure. Lower is better.

30k steps, rFID improves from 22.36 at 1 step down to 13.56 at 16 steps, demonstrating that the flow-based decoder benefits substantially from finer ODE integration. All configurations converge rapidly, indicating that RAC achieves stable reconstruction behavior within a modest training budget.

### Decoding Steps vs. Reconstruction Quality.

Figure 7 investigates how the number of inference steps in the RAC decoding process affects reconstruction quality (rFID) over the course of training. We conduct this analysis on a lightweight SD-VAE variant structure as a controlled quick test, evaluating four inference step configurations: 1-16 training steps, measured at 10-30k training steps. As expected, increasing the number of decoding steps consistently improves rFID across all training checkpoints, with the gap between 1-step and 16-step decoding being most pronounced at early training stages. By 30k steps, rFID improves from 22.36 at 1 step down to 13.56 at 16 steps, demonstrating that the flow-based decoder benefits substantially from finer ODE integration. All configurations converge rapidly, indicating that RAC achieves stable reconstruction behavior within a modest training budget.



**Fig. 8: Generative Decoding under Ultra-short Training:** To visually demonstrate the benefits of our generative decoding on the results, we only trained for 1k steps (this is merely 1/10k of the full training duration in other works), and then we observed the number of decoding inferences. It’s clearly see that during the initial training phase, multi-step decoding significantly contributed to the improvement in quality.

## 4.2 Generation Quality

**Generated Image Samples.** Figure 8 illustrates generative decoded image samples under ultra-short training (1k steps, 1/10k of full training duration), comparing 1-8 step generative decoding across diverse ImageNet categories. Even at this early training stage, the multi-step decoding of RAC progressively refines image quality: 1-step outputs capture coarse structure and semantics, while 4-step and 8-step inferences recover finer textures, sharper edges, and more faithful color rendition. This behavior demonstrates that RAC’s generative decoder functions as an iterative refinement mechanism, effectively compensating for the limited encoder training by leveraging the diffusion prior to denoise and enhance latent representations at inference time.

**Generation Quality Comparison.** Table 2 presents a quantitative comparison of RAC against baseline SiT models [18] and REPA-E [15]. RAC consistently achieves lower gFID and sFID scores while improving Inception Score (IS) and Precision across all scales, demonstrating that the rectified autoencoder with consistency path provides complementary benefits on top of existing representation alignment strategies. Specifically, RAC reduces gFID by 2.7, 1.6, and 1.6 points over REPA-E for SiT-B, SiT-L, and SiT-XL respectively, while maintaining competitive Recall.

**Table 2: Model scale comparison on ImageNet 256×256.** Our RAC improves generation quality across all model scales, achieving consistent gFID reductions over both the vanilla baseline and REPA-E.

Diff. Model	gFID↓	sFID↓	IS↑	Prec.↑	Rec.↑
SiT-B (130M)	49.5	7.00	27.5	0.46	<b>0.59</b>
+REPA-E	34.8	6.31	39.1	0.57	0.59
<b>+RAC (Ours)</b>	<b>32.1</b>	<b>6.18</b>	<b>41.3</b>	<b>0.59</b>	<b>0.60</b>
SiT-L (458M)	24.1	6.25	55.7	0.62	<b>0.60</b>
+REPA-E	16.3	5.69	75.0	0.68	0.60
<b>+RAC (Ours)</b>	<b>14.7</b>	<b>5.51</b>	<b>78.4</b>	<b>0.70</b>	<b>0.61</b>
SiT-XL (675M)	19.4	6.06	67.4	0.64	<b>0.61</b>
+REPA-E	12.8	5.04	88.8	0.71	0.58
<b>+RAC (Ours)</b>	<b>11.2</b>	<b>4.87</b>	<b>92.5</b>	<b>0.73</b>	<b>0.61</b>

These results confirm that RAC’s improvements are not model-capacity-specific but scale consistently, making it a broadly applicable enhancement to rectified flow-based generative frameworks.

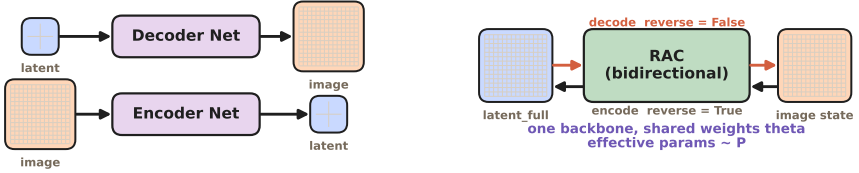


**Fig. 9: Parameter Efficiency of Bidirectional Design.** A conventional VAE-style bidirectional model uses separate encoder and decoder backbones to map between compact latent and image spaces. In contrast, RAC uses a single shared bidirectional model in the full-resolution state space, achieving encoding and decoding by reversing the flow direction rather than duplicating the backbone.

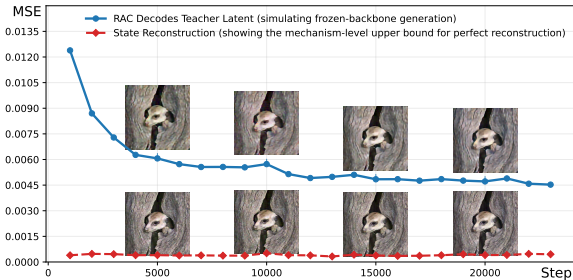


**Fig. 10: Encoding and Decoding Trajectory Symmetry.** Left: RAC decodes the full-resolution state to the image through a sequence of intermediate states. Right: the trajectories of sampled spatial positions are projected to a 2D PCA space, revealing that the decoding process follows structured and coordinated paths in the learned state space rather than independent pixel-wise changes.

### 4.3 Bidirectional Consistency

**Parameter Efficiency of Bidirectional Design.** As illustrated in Fig. 9, a conventional VAE-style bidirectional design relies on two separate networks: a decoder that maps a compact latent to image space and an encoder that maps the image back to the compact latent. This design achieves bidirectionality by duplicating the backbone across two directions. In contrast, RAC uses a single shared bidirectional model operating in the full-resolution state space. Encoding and decoding are both realized by the same model, with the transformation direction controlled by reversing the flow direction. This shared design avoids the need for a dedicated encoder-decoder pair and therefore provides a substantially more parameter-efficient bidirectional formulation.

**Encoding and Decoding Trajectory Symmetry.** As shown in Fig. 10, RAC does not transform the representation by a single abrupt jump from latent-like initialization to the final image. Instead, the model evolves the sample through a sequence of full-resolution intermediate states, producing a smooth decoding trajectory in the shared state space. The left panel visualizes this evolution directly in image space, where the representation gradually acquires semantic structure and local detail over time. The right panel further projects the trajectories of sampled spatial positions into a 2D PCA space. Although each sampled position corresponds to a fixed spatial location, its feature vector follows a coherent trajectory rather than remaining static or changing independently. Our model does not require two unrelated transformations for encoding and decoding, but instead traverses a common representation manifold in opposite directions.



**Our learning mechanism is unique:** With only 100 training steps, the state reconstruction achieves extremely high quality.

**Table 3: Mechanism-level ability of RAC.** Left: reconstruction errors during training. Decoding teacher latents with RAC simulates frozen-backbone generation, while state reconstruction measures the upper bound of reconstruction within RAC’s shared full-resolution state space. Right: qualitative state reconstruction examples.

#### 4.4 Generation–Reconstruction Gap Analysis

**Generation–Reconstruction Gap Analysis.** As shown in Table. 3, RAE [35] and Flux vae [13,14] achieve better results by increasing the number of channels and enhancing the expression ability of variables. However, if the state representation is used for training, it can learn a high-dimensional space without information loss. At this point, it is almost equivalent to fixed reconstruction learning generation. We can clearly see in the line graph that the generation ability is weaker than the reconstruction. This directly confirms our assumption in the Introduction and indicates that we have discovered in the mechanism how to unify generation and reconstruction with a training objective.

**Quantitative Gap between Generation and Reconstruction.** As shown in Table. 3 (Right), With just 100 steps, our state reconstruction is nearly perfect (of course, in normal use, encoded state condensed variables should be used, which is equivalent to a traditional compression with variable size). This is because our training builds a high-dimensional space starting from the image itself, and it can almost stabilize back to the pixel dimension. Even though this Latent space is not perfect, it does not affect the high performance of the reconstruction.

Method	gFID↓	sFID↓	IS↑	Prec.↑	Rec.↑
100K Iterations (20 Epochs)					
REPA [33]	19.40	6.06	67.4	0.64	<b>0.61</b>
REPA-E (scratch)	14.12	7.87	83.5	0.70	0.59
RAC (scratch, 1-step)	14.05	7.83	83.9	0.70	0.61
<b>RAC (scratch, 4-step)</b>	<b>13.47</b>	<b>7.31</b>	<b>86.2</b>	<b>0.71</b>	0.61

**Table 4: Ablation Study:** We ablate the key components of RAC under 100K iterations of end-to-end training from scratch, evaluating their individual contributions to generation quality.

#### 4.5 Ablation Study

**Ablation Study on RAC Components.** Table. 4 suggest that even RAC minimal consistency regularization is sufficient to preserve latent quality. Increasing to 4 steps yields further improvements across all metrics, validating that multi-step path consistency progressively refines the learned latent space without requiring any additional pretrained initialization.

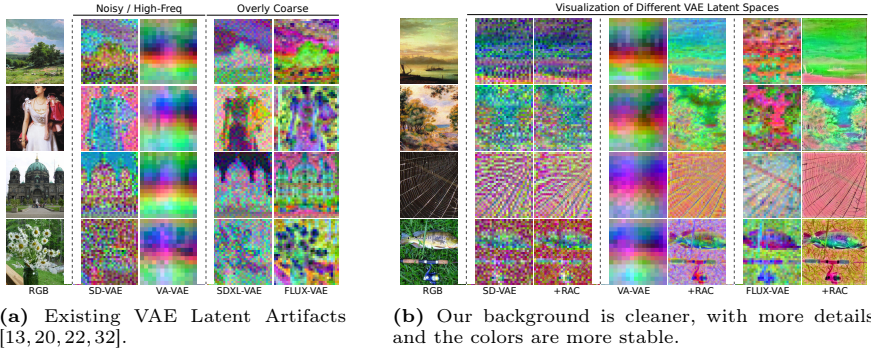


**Fig. 11:** The existing baseline latent manifolds show architecture-dependent anisotropy, where principal components are dominated by either stochastic high-frequency texture or coarse low-frequency blocks instead of semantic structure. RAC consistently re-allocates variance to spatially coherent components, yielding cleaner, more content-aligned latent geometry while preserving scene identity, which suggests improved cross-architecture latent regularity.

## 4.6 Latent Space Analysis

**Latent Space PCA Visualization.** Figure 11 highlights two complementary observations. First, different pretrained VAE architectures produce latent spaces with distinct but systematic defects: some are dominated by noisy high-frequency patterns, whereas others collapse fine details into coarse, low-information structures. Second, RAC-enhanced representations substantially regularize these latent distributions, suggesting that RAC improves latent quality as a general refinement mechanism rather than a backbone-specific trick.

## 5 Conclusion

This paper introduces RAC (Rectified Flow Auto Coder), an automatic encoding framework based on rectified flow, aiming to fundamentally solve the problem of inconsistency between generation and reconstruction in traditional VAEs. Unlike traditional VAEs which treat decoding as a single-step mapping, RAC models the decoding process as a continuous-time velocity field integration, enabling the model to gradually correct latent variables along the decoding path, thereby significantly reducing the performance gap between generation and reconstruction. Thanks to the time reversal mechanism, RAC naturally supports bidirectional inference, that is, the same velocity field model can simultaneously perform encoding and decoding functions, reducing the parameter quantity by nearly 41%. We designed a joint training objective including path consistency loss, latent variable alignment loss, and reconstruction constraints, ensuring the quality of reconstruction while enhancing the generation ability. Experimental results show that RAC outperforms existing SOTA VAEs in terms of both reconstruction and generation performance, but with approximately 70% lower computational cost.

## References

1. Chen, R.T.Q., Rubanova, Y., Bettencourt, J., Duvenaud, D.K.: Neural ordinary differential equations. In: Bengio, S., Wallach, H., Larochelle, H., Grauman, K., Cesa-Bianchi, N., Garnett, R. (eds.) *Advances in Neural Information Processing Systems*. vol. 31. Curran Associates, Inc. (2018), [https://proceedings.neurips.cc/paper\\_files/paper/2018/file/69386f6bb1dfed68692a24c8686939b9-Paper.pdf](https://proceedings.neurips.cc/paper_files/paper/2018/file/69386f6bb1dfed68692a24c8686939b9-Paper.pdf)
2. Deng, J., Dong, W., Socher, R., Li, L.J., Li, K., Fei-Fei, L.: Imagenet: A large-scale hierarchical image database. In: *2009 IEEE conference on computer vision and pattern recognition*. pp. 248–255. Ieee (2009)
3. Dinh, L., Sohl-Dickstein, J., Bengio, S.: Density estimation using real NVP. In: *International Conference on Learning Representations* (2017), <https://openreview.net/forum?id=HkpbnH9lx>
4. Esser, P., Rombach, R., Ommer, B.: Taming transformers for high-resolution image synthesis. In: *Proceedings of the IEEE/CVF Conference on Computer Vision and Pattern Recognition (CVPR)*. pp. 12873–12883 (June 2021)
5. Fang, S., Chen, C., Wang, L., Zheng, C., Sui, C., Tian, Y.: Signllm: Sign language production large language models. In: *Proceedings of the IEEE/CVF International Conference on Computer Vision (ICCV) Workshops*. pp. 6622–6634 (October 2025)
6. Fang, S., Feng, Y., Sui, C., Zhong, H., Yi, H., Metaxas, D.N.: Signx: Continuous sign recognition in compact pose-rich latent space (2026), <https://arxiv.org/abs/2504.16315>
7. Fang, S., Feng, Y., Zhong, H., Zhang, Y., Metaxas, D.N.: Stable signer: Hierarchical sign language generative model (2026), <https://arxiv.org/abs/2512.04048>
8. Fang, S., Sui, C., Zhou, Y., Zhang, X., Zhong, H., Tian, Y., Chen, C.: Signdiff: Diffusion model for american sign language production. In: *2025 IEEE 19th International Conference on Automatic Face and Gesture Recognition (FG)*. pp. 1–11 (2025). <https://doi.org/10.1109/FG61629.2025.11099440>
9. Fang, S., Zhong, H., Feng, Y., Zhang, Y., Metaxas, D.N.: Streamflow: Theory, algorithm, and implementation for high-efficiency rectified flow generation (2026), <https://arxiv.org/abs/2511.22009>
10. Kingma, D.P., Welling, M.: Auto-encoding variational bayes. *arXiv preprint arXiv:1312.6114* (2013)
11. Kingma, D.P., Dhariwal, P.: Glow: Generative flow with invertible 1x1 convolutions. In: Bengio, S., Wallach, H., Larochelle, H., Grauman, K., Cesa-Bianchi, N., Garnett, R. (eds.) *Advances in Neural Information Processing Systems*. vol. 31. Curran Associates, Inc. (2018), [https://proceedings.neurips.cc/paper\\_files/paper/2018/file/d139db6a236200b21cc7f752979132d0-Paper.pdf](https://proceedings.neurips.cc/paper_files/paper/2018/file/d139db6a236200b21cc7f752979132d0-Paper.pdf)
12. Kouzelis, T., Kakogeorgiou, I., Gidaris, S., Komodakis, N.: Eq-vae: Equivariance regularized latent space for improved generative image modeling. *arXiv preprint arXiv:2502.09509* (2025)
13. Labs, B.F.: Flux. <https://github.com/black-forest-labs/flux> (2024)
14. Labs, B.F., Batifol, S., Blattmann, A., Boesel, F., Consul, S., Diagne, C., Dockhorn, T., English, J., English, Z., Esser, P., Kulal, S., Lacey, K., Levi, Y., Li, C., Lorenz, D., Müller, J., Podell, D., Rombach, R., Saini, H., Sauer, A., Smith, L.: Flux.1 kontext: Flow matching for in-context image generation and editing in latent space (2025), <https://arxiv.org/abs/2506.15742>
15. Leng, X., Singh, J., Hou, Y., Xing, Z., Xie, S., Zheng, L.: Repa-e: Unlocking vae for end-to-end tuning with latent diffusion transformers (2025), <https://arxiv.org/abs/2504.10483>

16. Lipman, Y., Chen, R.T.Q., Ben-Hamu, H., Nickel, M., Le, M.: Flow matching for generative modeling. In: The Eleventh International Conference on Learning Representations (2023), <https://openreview.net/forum?id=PqvMRDCJT9t>
17. Liu, X., Gong, C., qiang liu: Flow straight and fast: Learning to generate and transfer data with rectified flow. In: The Eleventh International Conference on Learning Representations (2023), <https://openreview.net/forum?id=XVjTT1nw5z>
18. Ma, N., Goldstein, M., Albergo, M.S., Boffi, N.M., Vanden-Eijnden, E., Xie, S.: Sit: Exploring flow and diffusion-based generative models with scalable interpolant transformers. In: European Conference on Computer Vision. pp. 23–40. Springer (2024)
19. Peebles, W., Xie, S.: Scalable diffusion models with transformers. In: 2023 IEEE/CVF International Conference on Computer Vision (ICCV). pp. 4172–4182 (2023). <https://doi.org/10.1109/ICCV51070.2023.00387>
20. Podell, D., English, Z., Lacey, K., Blattmann, A., Dockhorn, T., Müller, J., Penna, J., Rombach, R.: SDXL: Improving latent diffusion models for high-resolution image synthesis. In: The Twelfth International Conference on Learning Representations (2024), <https://openreview.net/forum?id=di52zR8xgf>
21. Rombach, R., Blattmann, A., Lorenz, D., Esser, P., Ommer, B.: High-resolution image synthesis with latent diffusion models. In: Proceedings of the IEEE/CVF Conference on Computer Vision and Pattern Recognition (CVPR). pp. 10684–10695 (June 2022)
22. Rombach, R., Blattmann, A., Lorenz, D., Esser, P., Ommer, B.: High-resolution image synthesis with latent diffusion models. In: Proceedings of the IEEE/CVF conference on computer vision and pattern recognition. pp. 10684–10695 (2022)
23. Ronneberger, O., Fischer, P., Brox, T.: U-net: Convolutional networks for biomedical image segmentation. In: Navab, N., Hornegger, J., Wells, W.M., Frangi, A.F. (eds.) Medical Image Computing and Computer-Assisted Intervention – MICCAI 2015. pp. 234–241. Springer International Publishing, Cham (2015)
24. Salimans, T., Ho, J.: Progressive distillation for fast sampling of diffusion models. In: International Conference on Learning Representations (2022), <https://openreview.net/forum?id=TIIXIpzhoI>
25. Shu, D., Wu, X., Zhao, H., Rai, D., Yao, Z., Liu, N., Du, M.: A survey on sparse autoencoders: Interpreting the internal mechanisms of large language models. In: Christodoulopoulos, C., Chakraborty, T., Rose, C., Peng, V. (eds.) Findings of the Association for Computational Linguistics: EMNLP 2025. pp. 1690–1712. Association for Computational Linguistics, Suzhou, China (Nov 2025). <https://doi.org/10.18653/v1/2025.findings-emnlp.89>, <https://aclanthology.org/2025.findings-emnlp.89/>
26. Song, Y., Dhariwal, P., Chen, M., Sutskever, I.: Consistency models. In: Krause, A., Brunskill, E., Cho, K., Engelhardt, B., Sabato, S., Scarlett, J. (eds.) Proceedings of the 40th International Conference on Machine Learning. Proceedings of Machine Learning Research, vol. 202, pp. 32211–32252. PMLR (23–29 Jul 2023), <https://proceedings.mlr.press/v202/song23a.html>
27. Song, Y., Sohl-Dickstein, J., Kingma, D.P., Kumar, A., Ermon, S., Poole, B.: Score-based generative modeling through stochastic differential equations. In: International Conference on Learning Representations (2021), <https://openreview.net/forum?id=PxTIG12RRHS>
28. Vahdat, A., Kautz, J.: Nvae: A deep hierarchical variational autoencoder. In: Larochelle, H., Ranzato, M., Hadsell, R., Balcan, M., Lin, H. (eds.) Advances in

- Neural Information Processing Systems. vol. 33, pp. 19667–19679. Curran Associates, Inc. (2020), [https://proceedings.neurips.cc/paper\\_files/paper/2020/file/e3b21256183cf7c2c7a66be163579d37-Paper.pdf](https://proceedings.neurips.cc/paper_files/paper/2020/file/e3b21256183cf7c2c7a66be163579d37-Paper.pdf)
29. Wang, M., Jiang, D., Li, L., Lin, Y., Shen, G., Kong, X., Liu, Y., Dai, G., Wang, J.: Vae-repa: Variational autoencoder representation alignment for efficient diffusion training (2026), <https://arxiv.org/abs/2601.17830>
  30. Yan, C., Liu, S., Liu, H., Peng, X., Wang, X., Chen, F., Fu, L., Mei, X.: Hybrid sd: Edge-cloud collaborative inference for stable diffusion models (2024), <https://arxiv.org/abs/2408.06646>
  31. Yao, J., Wang, X.: Reconstruction vs. generation: Taming optimization dilemma in latent diffusion models. arXiv preprint arXiv:2501.01423 (2025)
  32. Yao, J., Yang, B., Wang, X.: Reconstruction vs. generation: Taming optimization dilemma in latent diffusion models. In: Proceedings of the IEEE/CVF Conference on Computer Vision and Pattern Recognition (2025)
  33. Yu, S., Kwak, S., Jang, H., Jeong, J., Huang, J., Shin, J., Xie, S.: Representation alignment for generation: Training diffusion transformers is easier than you think. arXiv preprint arXiv:2410.06940 (2024)
  34. Zhai, S., ZHANG, R., Nakkiran, P., Berthelot, D., Gu, J., Zheng, H., Chen, T., Bautista, M.Á., Jaitly, N., Susskind, J.M.: Normalizing flows are capable generative models. In: Forty-second International Conference on Machine Learning (2025), <https://openreview.net/forum?id=2uheUFcFsM>
  35. Zheng, B., Ma, N., Tong, S., Xie, S.: Diffusion transformers with representation autoencoders. In: The Fourteenth International Conference on Learning Representations (2026), <https://openreview.net/forum?id=0u1LigJaab>
  36. Zhuang, X., Xie, Y., Deng, Y., Liang, L., Ru, J., Yin, Y., Zou, Y.: Vargpt: Unified understanding and generation in a visual autoregressive multimodal large language model (2025), <https://arxiv.org/abs/2501.12327>